Journal of Power Sources 258 (2014) 314–320

Contents lists available at ScienceDirect

Journal of Power Sources

journal homepage: www.elsevier.com/locate/jpowsour

Short communication

# Structural and electrochemical stability of Li-rich layer structured $Li_2MoO_3$ in air

Jun Ma, Yurui Gao, Zhaoxiang Wang*, Liquan Chen

*Key Laboratory for Renewable Energy, Beijing Key Laboratory for New Energy Materials and Devices, Beijing National Laboratory for Condensed Matter Physics, Institute of Physics, Chinese Academy of Sciences, PO Box 603, Beijing 100190, China*

## HIGHLIGHTS

- $Li_2MoO_3$ is synthesized as a component for constructing Li-rich cathodes.
- Long-term air exposure degrades the surface structure and performance of $Li_2MoO_3$.
- Surface reaction is limited with 30 nm in depth during long-term air exposure.
- $Li_2MoO_3$ has high structural stability despite the surface reaction in air.
- The aging mechanism of $Li_2MoO_3$ in air is suggested.

## GRAPHICAL ABSTRACT

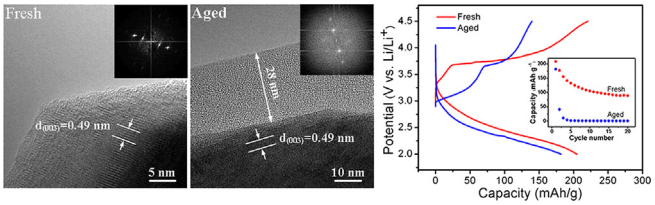


## ARTICLE INFO

*Article history:*
Received 20 December 2013
Accepted 15 February 2014
Available online 25 February 2014

*Keywords:*
Lithium-rich cathode materials
Layer structure
Aging
Stability
Cycling performance

## ABSTRACT

$Li_2MnO_3$ is an important component of the Li-rich Mn-based high-capacity cathode material for lithium ion batteries, $xLi_2MnO_3\cdot(1-x)LiMO_2$ composites. Replacing $Li_2MnO_3$ with iso-structured $Li_2MoO_3$ is expected to improve the rate performance and suppress the oxygen release of the composites at high potentials due to the higher electric conductivity of $Li_2MoO_3$ and its more facile charge compensation (by $Mo^{4+}/Mo^{6+}$ redox) upon Li removal than that of $Li_2MnO_3$. As part of our series work on the $Li_2MoO_3$-based Li-rich layer structured cathode materials, this article is to study the structural and performance stability of $Li_2MoO_3$ in air. The obtained information will shed light on the development and application of $xLi_2MoO_3\cdot(1-x)LiMO_2$ composite cathode materials though $Li_2MoO_3$ will not be applied as an independent cathode material.

© 2014 Elsevier B.V. All rights reserved.

## 1. Introduction

Energy density is one of the vital criteria to meet for applications of lithium ion batteries in portable devices and electric vehicles. Among all the current cathode materials, $Li_2MnO_3$-based Li-rich layer structured oxides $xLi_2MnO_3\cdot(1-x)LiMO_2$ ($M$ = Mn, Ni, Co, *etc.*) are the most attractive owing to their high reversible capacities over 280 mAh $g^{-1}$ at room temperature [1,2]. Such high capacities are attributed to the presence of $Li_2MnO_3$ and its structure-stabilizing effect to the $LiMO_2$ phase [3,4]. However, the reaction mechanisms of these Li-rich oxides are still in argument due to their complicated structures and the incomplete understanding to the electrochemical activity of $Mn^{4+}$ ions in $Li_2MnO_3$ [5,6]. To resolve these issues, other Li-rich layered oxides $Li_2MO_3$ ($M$ = Ti, Zr, Ru, Sn, *etc.*) have been studied [7–10]. On the other hand, the oxygen evolution of $Li_2MnO_3$ at high charge potentials and its intrinsically low conductivity lead to safety concerns, structural degradation and poor rate performance of the $Li_2MnO_3$-based composites [11]. Thus, searching for substituent of $Li_2MnO_3$ with

* Corresponding author. Tel.: +86 10 82649050; fax: +86 10 82649046.
*E-mail address:* zxwang@iphy.ac.cn (Z. Wang).

http://dx.doi.org/10.1016/j.jpowsour.2014.02.056
0378-7753/© 2014 Elsevier B.V. All rights reserved.

high conductivity and free of oxygen release in Li-rich layered oxide electrodes becomes essential to enhance their electrochemical performances.

$Li_2MoO_3$ has a theoretical $Li^+$ extraction/insertion capacity of 339 mAh $g^{-1}$ simply by a single $Mo^{4+}/Mo^{6+}$ redox reaction [12–17]. In comparison, any lithium extraction from $Li_2MnO_3$ will lead to oxidation of its oxygen ($O_2$ release) and irreversible structural degradation. Similar to $Li_2MnO_3$, $Li_2MoO_3$ also consists of alternative Li layers and randomly distributed [$Li_{1/3}Mo_{2/3}$] layers [14–16], as is shown in Fig. 1. X-ray and neutron diffraction studies show that it has a disordered $NaFeO_2$ structure ($R\bar{3}m$; $a$ = 2.884 Å, $c$ = 14.834 Å) with the Mo ions present as $Mo_3O_{13}$ clusters in the [$Li_{1/3}Mo_{2/3}$] layer. In addition, the electric conductivity of $Li_2MoO_3$ (black in color) should be higher than that of $Li_2MnO_3$ (red) based on their colors. Therefore, $Li_2MoO_3$ and its related oxides can be alternate building blocks of Li-rich layer structured cathode materials with higher safety and better rate performances than the current $Li_2MnO_3$-based ones. Furthermore, the simple composition and single $Mo^{4+}/Mo^{6+}$ redox reaction in $Li_2MoO_3$ are beneficial for understanding the reaction mechanism of the complicated Li-rich layered oxide electrode materials. Actually our comprehensive studies, theoretical and experimental, have shown that $Li_2MoO_3$ can indeed be used to construct Li-rich high-capacity cathode materials (submitted and/or to be published elsewhere).

On the other hand, the stability of the Li-rich layered oxides during storage has not received sufficient attention. Indeed, the storage characteristics of the electrode materials have significant impacts on their structure and electrochemical performances [18–24]. Zhao et al. [23] reported that the capacity of the cathode materials decays due to formation of $Li_2CO_3$ on the particle surface. We previously reported that commercial $LiFePO_4$ could be oxidized in humid and/or hot air and became α-$Fe_2O_3$ and $FePO_4$ [18]. More recently, we studied the stability of $Li_4Ti_5O_{12}$ anode material in air [25]. First-principles calculations indicate that $Li_4Ti_5O_{12}$ is lithium-truncated at the surface, beneficial for protecting the internal structure from air attack. As $Mo^{4+}$ is less stable than $Mo^{6+}$ in air and the $CO_2$ is likely to be adsorbed on the surface of $Li_2MoO_3$ and react with $Li^+$, the stability of $Li_2MoO_3$ in air becomes an important topic to the application of $Li_2MoO_3$-based ($xLi_2MoO_3\cdot(1-x)LiM'O_2$) Li-rich cathode materials.

In this work, we evaluate the structural and electrochemical stability of $Li_2MoO_3$ in air at room temperature and explore its aging mechanism. The findings here will shed light on the development and application of the $Li_2MoO_3$-based Li-rich cathode materials though $Li_2MoO_3$ itself will not be used as an independent cathode material in practice.

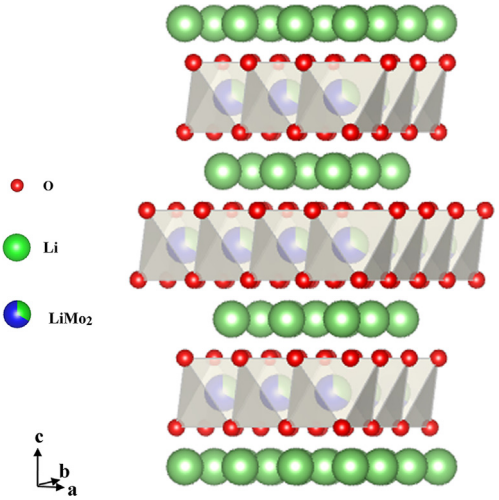


**Fig. 1.** Lattice structure of $Li_2MoO_3$.

## 2. Experimental

Phase-pure $Li_2MoO_3$ powder was prepared by reducing commercial $Li_2MoO_4$ (Alfa Aesar) at 650 °C for 24 h in flowing $H_2$/Ar (10:90 v/v). The aged $Li_2MoO_3$ was obtained by storing the fresh sample in desiccators (the relative humidity is below 10%) at room temperature for 120 days. The structure of the $Li_2MoO_3$ powder was characterized on an X'Pert Pro MPD X-ray diffractometer (XRD, Philips, Holland) with monochromatized Cu Kα radiation ($\lambda$ = 1.5405 Å). The morphology and microstructure were observed on a scanning electron microscope (SEM, Hitachi S-4800) and high resolution transmission electron microscope (HRTEM, Tecnai G2 F20 U-TWIN), respectively. The chemical state of the Mo ions in $Li_2MoO_3$ was identified using X-ray photoelectron spectroscopy (XPS, ESCALAB250, Thermo, USA). The binding energy was calibrated with C1s (284.8 eV) of contaminated carbon in the vacuum chamber. Each Fourier transformed infrared (FTIR) spectrum was the average of 400 scans on VERTEX 70 V FTIR spectrometer (Bruker, Germany). The material for the FTIR test was mixed with dry KBr powder and pressed to pellets. Raman spectroscopy was conducted on Horiba/Jobin Yvon HR800 (France) using the 532 nm laser line.

The electrochemical test of the prepared $Li_2MoO_3$ and commercial $Li_2MoO_4$, $MoO_3$, and $Li_2CO_3$ were performed as follows. Electrode sheets were fabricated by coating the slurry containing 80 wt% active materials, 10 wt% acetylene black and 10 wt% polyvinylidene fluoride dissolved in *N*-methyl-2-pyrrolidone on a roughened Al foil. Test cells were assembled in an Ar-filled glove box using Li metal as the counter electrode, Celgard 2300 as the separator, and 1.0 mol $L^{-1}$ $LiPF_6$ dissolved in ethylene carbonate/dimethyl carbonate (EC:DEC = 1:1 v/v) as the electrolyte. The cells were galvanostatically charged and discharged at room temperature at a current density of 10 mA $g^{-1}$ between 2.0 and 4.5 V *vs.* $Li/Li^+$.

## 3. Results and discussion

### 3.1. Structural characterization

XRD study shows no detectable structural difference between the fresh and aged $Li_2MoO_3$ (Fig. 2). The sharp peaks reveal that our $Li_2MoO_3$ is well crystallized. The diffraction peaks of both samples can be indexed to a trigonal unit cell with the space group of $R\bar{3}m$. Unlike $Li_2MnO_3$, no diffraction peaks between 20 and 25° can be observed due to random distribution of the Li (1/3) and Mo (2/3) ions in the transition metal (Mo) layers [12–15]. The splitting of the

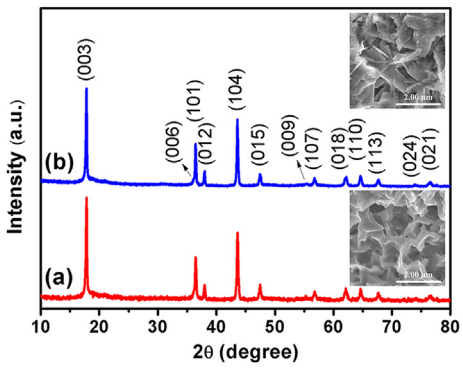


**Fig. 2.** XRD patterns of (a) fresh and (b) aged $Li_2MoO_3$. The insets are for their corresponding morphologies.

(018)/(110) doublet and the intensity ratio of the (003)/(104) diffraction lines are usually used to evaluate the crystallinity and the degree of Li–Mo antisites, respectively [26,27]. The clear splitting of the (018)/(110) doublet of both samples indicates that the well-defined layer structure of $Li_2MoO_3$ remains even after long-term exposure to air. The intensity ratio of the (003)/(104) diffraction lines for the fresh and aged $Li_2MoO_3$ is about 1.49 and 1.16, respectively. The decreased intensity ratio implies the increase of the Li–Mo antisites in the aged $Li_2MoO_3$. As more $Mo^{4+}$ ions migrate from the $[Li_{1/3}Mo_{2/3}]$ layer into the Li layer, the $Mo_3O_{13}$ clusters in the $[Li_{1/3}Mo_{2/3}]$ layers will be disaggregated and the local coordination environment of the $Li^+$ and $Mo^{4+}$ ions will be changed. This variation may influence the diffusion of the $Li^+$ ions during electrochemical (de)lithiation.

SEM imaging (insets of Fig. 2) shows that the $Li_2MoO_3$ particles are irregular aggregates, varying from a few to tens of micrometers in size. The aggregates are randomly accumulated nanosheets. Air exposure does not change their morphology.

As XRD shows only the average structure of the crystallized species, HRTEM is used to investigate whether or not amorphous species are formed on the surface of the aged $Li_2MoO_3$. The HRTEM images of the fresh and aged $Li_2MoO_3$ are compared in Fig. 3. Clear and intact lattice fringes are found extended to the edge of the crystallite for the fresh $Li_2MoO_3$. In contrast, a thick (*ca.* 28 nm) and continuous amorphous layer covers the surface of the aged $Li_2MoO_3$ (Fig. 3(b)). Below the amorphous layer, the lattice fringe is clear but divided into many small domains with some defects, bent lattice fringes and disordered regions. The amorphous surface and

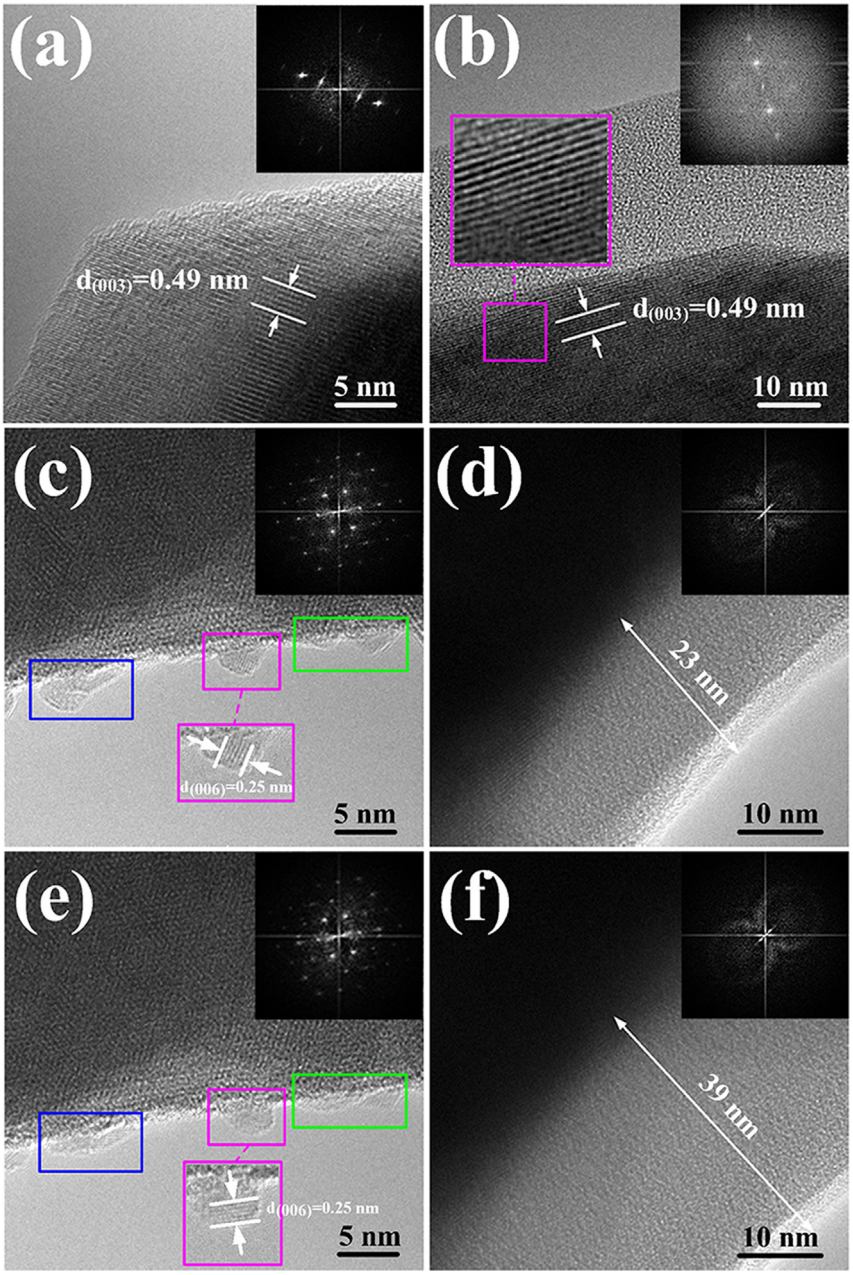


**Fig. 3.** HRTEM images of (a) fresh and (b) aged $Li_2MoO_3$ at [010] zone axis; evolution of the same area for the fresh and aged $Li_2MoO_3$ under continuous electron beam irradiation at [001] zone axis (c *vs.* e and d *vs.* f). The insets are for the corresponding SAED patterns.

damaged lattice fringe indicate the defected surface of the aged $Li_2MoO_3$. Consistent with the HRTEM imaging, selected-area electron diffraction (SAED) analysis shows that the fresh and aged $Li_2MoO_3$ have a typical rhombohedral symmetry with $d_{(003)}$ spacing of *ca.* 0.49 nm (Fig. 3(a) and (b)).

It is interesting that, under continuous electron beam irradiation for a few seconds, the surface of the aged and on the fresh $Li_2MoO_3$ surface reveals different behaviors. Small crystallite humps appear on the surface of fresh $Li_2MoO_3$ (Fig. 3(c)). These humps are recognized to be $Li_2MoO_3$ (006) facets with $d_{(006)}$ spacing of *ca.* 0.25 nm. Although the $Li_2MoO_3$ (006) diffraction line is quite faint in the XRD pattern of the fresh sample, the (006) facets show clear lattice fringes in the HRTEM image. This phenomenon seems to be related with the Li–Mo antisites, induced with the electron beam irradiation and due to their similarity in ionic radius (0.68 Å for $Li^+$ [28] *vs.* 0.65 Å for $Mo^{4+}$ [29]). The size and orientation of these humps vary as they grow upon continuous electron irradiation (Fig. 3(e)). No amorphous layer can be observed on the surface in this process; the structure of the $Li_2MoO_3$ bulk remains unchanged too (inset SAED pattern in each). This means that the reaction only occurs on or near the surface of $Li_2MoO_3$ (a depth of 25–30 nm) though it has long been exposed to air. Nevertheless, the amorphous layer on the surface of the aged $Li_2MoO_3$ is quite unstable under continuous electron beam irradiation. Its thickness increases from about 23 nm to more than 39 nm in a few seconds (Fig. 3(d) *vs.* (f)). In addition, almost no crystalline features can be observed in the bulk (insets in Fig. 3(d) and (f)), probably due to the disturbance of the thick amorphous layer to the observation. Clearly air exposure leads to changes in surface morphology and properties of $Li_2MoO_3$, and probably surface reactions on it.

### 3.2. Recognition of surface reaction products

Surface sensitive XPS was first employed to compare the oxidation state of the Mo ions on the surface of fresh and aged $Li_2MoO_3$ (Fig. 4). Due to the partial overlapping of the Mo $3d_{3/2}$ peak of one oxidation state with the Mo $3d_{5/2}$ peak of another state, only three peaks (rather than two or two pairs) can be recognized around 230.0, 232.8 and 235.6 eV in the spectra of both the fresh and aged $Li_2MoO_3$ (with different relative intensities, of course). By means of peak splitting, two pairs of peaks with Mo $3d_{5/2}$ binding energy at 230.1 and 232.7 eV are resolved in the spectrum of fresh $Li_2MoO_3$; they are assigned to $Mo^{4+}$ and $Mo^{6+}$, respectively [30,31]. In the spectrum of the aged sample, three pairs of peaks with Mo $3d_{5/2}$ binding energies of about 230.5, 230.9 and 232.7 eV are assigned to $Mo^{4+}$, $Mo^{\sigma+}$ ($5 < \sigma < 6$) and $Mo^{6+}$, respectively [30,31]. Furthermore, the variation of the relative intensities of the Mo 3d peaks suggests that $Li_2MoO_3$ tend to be oxidized or decomposed after long-term air exposure and most of its $Mo^{4+}$ ions on the surface are oxidized, though no other crystalline species can be detected by XRD (Fig. 2) or recognized by HRTEM (Fig. 3), in the aged $Li_2MoO_3$.

FTIR and Raman spectroscopy that are sensitive to both crystalline and amorphous species are then conducted to recognize the materials in the aged $Li_2MoO_3$ (Fig. 5). The obvious peaks at 446, 497, 559 and 698 $cm^{-1}$ in the FTIR spectrum are attributed to $Li_2MoO_3$ [32]. By comparing the FTIR spectrum of the aged $Li_2MoO_3$ with that of some commercial reagents, we can easily recognize that $Li_2CO_3$, $Li_2MoO_4$ and $MoO_3$ are the reaction products on the air-exposed $Li_2MoO_3$. As no structural changes are observed below the amorphous layer in the HRTEM image, these species are believed to be the main composition of the amorphous layer in Fig. 3(b).

These assignments are supported with the Raman spectroscopy of commercial $Li_2CO_3$ (1087 $cm^{-1}$) and $Li_2MoO_4$ (841, 878, and 897 $cm^{-1}$). The broad Raman band at about 240 $cm^{-1}$ is attributed to the Mo–O–Mo bridging species in $Mo_3O_{13}$ clusters [33]. It tends to disappear after aging, consistent with the decrease of $Mo_3O_{13}$ clusters and the increased Li–Mo antisites. The broad band at 897 $cm^{-1}$ and weak band at 841 $cm^{-1}$ are ascribed to isolated tetrahedral coordinated $MoO_4$ species [34], while the band at 353 $cm^{-1}$ corresponds to Mo=O bond of octahedral coordinated $MoO_6$ species [33,35]. As for the aged $Li_2MoO_3$, the appearance of bands at 897 and 841 $cm^{-1}$ and the weakening of the band at 353 $cm^{-1}$ indicate that the $MoO_6$ octahedron distorts and transforms to $MoO_4$ tetrahedron, driven by the oxidation of $Mo^{4+}$ ions. Therefore, we confirm that $Li_2MoO_3$ is partially oxidized/decomposed to $Li_2CO_3$, $Li_2MoO_4$ and $MoO_3$. The oxidation of $Mo^{4+}$ to $Mo^{6+}$ ions changes the coordination environment of the $Mo^{4+}$ ions and distorts the $MoO_6$ octahedra. Therefore, the creation of the $Li^+$ vacancies and the distortion of the $MoO_6$ octahedra combine to become the driving force for the Mo ion migration, the damaged $Mo_3O_{13}$ clusters and the increased Li–Mo antisites in the aged $Li_2MoO_3$.

Combining the facts that reaction products can be recognized by crystallinity-insensitive FTIR and Raman spectroscopy but cannot be detected by crystallinity-sensitive XRD and HRTEM, the air-$Li_2MoO_3$ reaction is believed to be limited to the surface (a depth less than 30 nm) of $Li_2MoO_3$. Its structural integrity is maintained in the bulk though it is exposed to air for 120 days. These indicate that the structure of bulk $Li_2MoO_3$ is pretty stable in air though surface reactions can occur very quickly in the first few minutes exposing to air.

### 3.3. Electrochemical evaluation

Partial oxidation/decomposition of $Li_2MoO_3$ in air will still deteriorate its electrochemical performances. Compared with the

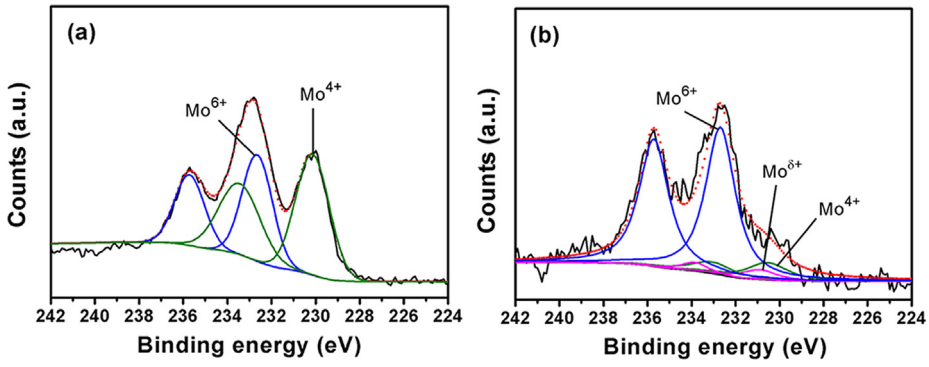


**Fig. 4.** Determination of the oxidation states of the Mo ions in (a) fresh and (b) aged $Li_2MoO_3$ by XPS spectra of Mo 3d.

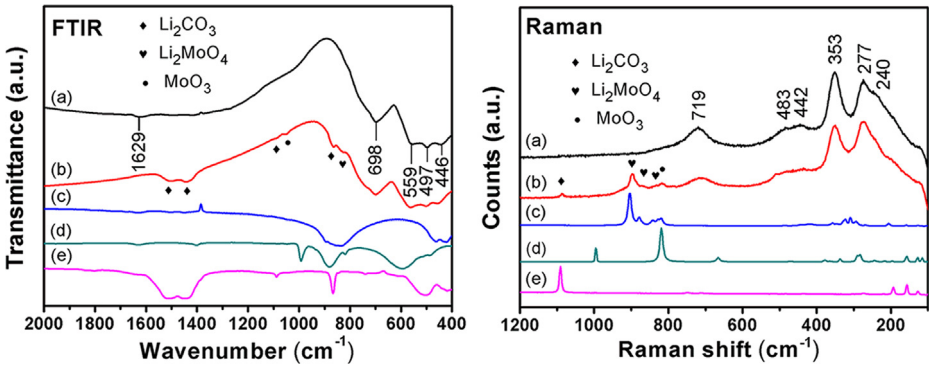


**Fig. 5.** FTIR and Raman spectra of (a) fresh and (b) aged $Li_2MoO_3$. The spectra of commercial (c) $Li_2MoO_4$, (d) $MoO_3$, and (e) $Li_2CO_3$ are recorded for reference.

fresh sample, the aged material has three features in the initial charge and discharge curves (Fig. 6(a)). (1) Both the charge and discharge capacities are lower than that of the fresh sample; (2) The charge capacity increases on the first plateau between 3.2 and 3.7 V but the capacity decreases on the second plateau above 3.7 V; (3) The potentials of both the charge and discharge plateaus become lower. The decayed charge capacity is attributed to the formation of $Li_2CO_3$ and $Li_2MoO_4$ because it consumes $Li^+$ ions but these two species are electrochemically inert between 2.0 and 4.5 V (Y.M. Zhao et al. found that the Li insertion capacity of their home-prepared $Li_2MoO_4$ is over 700 mAh $g^{-1}$ below 2.0 V but negligible above 2.0 V, according to private communication). In addition, their low electronic conductivity further hinders the charge transfer on the interface and leads to increased polarization [22,36]. The lowered charge plateau and increased charge capacity between 3.2 and 3.7 V seem to be related to the $Li^+$ vacancies created during the oxidation/decomposition of $Li_2MoO_3$. The enhanced Li–Mo antisites are believed to be responsible for the capacity decrease of the plateau above 3.7 V. Kobayashi et al. [12] believed that the arrangement of the $Mo_3O_{13}$ clusters in the $[Li_{1/3}Mo_{2/3}]$ layer of $Li_2MoO_3$, dependent on the synthesis temperature, affects the diffusion rate of the $Li^+$ ions, and therefore, the charge plateau of $Li_2MoO_3$. In this work, the $Mo_3O_{13}$ clusters are decomposed and Li–Mo antisites become much more severe in the aged $Li_2MoO_3$ than in the fresh sample. In addition, similar to the occurrence induced by electrochemical $Li^+$ extraction (to be published elsewhere), the chemical (here) $Li^+$ extraction from the Li layer (first-principles calculations indicates that it is more difficult to extract $Li^+$ ions from the $[Li_{1/3}Mo_{2/3}]$ layer than from the Li layer, data to be published elsewhere) creates $Li^+$ vacancies, promotes the $Mo^{4+}$ migration and the Li–Mo antisites. The increased number of the Mo ions in the Li sites as well as the strong interaction between the Mo and O ions will block $Li^+$ ion diffusion even at high potentials. As a result, the charge capacity of the aged $Li_2MoO_3$ above 3.7 V is lower than that of the fresh sample.

Fig. 6(a) also shows that the coulombic efficiency of the fresh $Li_2MoO_3$ reaches 98.9% but that of the aged $Li_2MoO_3$ should have reached 130.3% in the initial cycle. Li et al. [37] reported that the reactivity of $Li_2CO_3$ is nearly negligible between 4.3 and 2.0 V. Here we show that $Li_2CO_3$ and $Li_2MoO_4$ almost have no contribution to the charge capacity between 4.5 and 2.0 V (Fig. 6(b)). Thus, the extra capacity in the initial discharge of the aged $Li_2MoO_3$ should be assigned to the formation of $MoO_3$. In the subsequent cycles, the capacity of the aged $Li_2MoO_3$ decreases drastically (inset of Fig. 6(a)).

### 3.4. Aging mechanism

Fig. 7 schemes the aging mechanism of $Li_2MoO_3$ in air. Owing to the stability of $Mo^{6+}$ in air, $Li_2MoO_3$ tends to adsorb $O_2$ on its surface and is oxidized to $Li_2MoO_4$, accompanied with atom rearrangement

$$Li_2MoO_3 + 1/2O_2 \rightarrow Li_2MoO_4 \quad (1)$$

Meanwhile, the reaction of $Li_2MoO_3$ with $CO_2$ in air produces $Li_2CO_3$, consumes its $Li^+$ ions at or near the surface, leads to $Li^+$ diffusion from the bulk to the surface due to $Li^+$ concentration gradient, produces Li-insufficient $Li_{2-2x}MoO_3$ and finally $MoO_3$, with the help of oxygen (Equations (2) and (3))

$$Li_2MoO_3 + xCO_2 + x/2O_2 \rightarrow xLi_2CO_3 + Li_{2-2x}MoO_3 \quad (2)$$

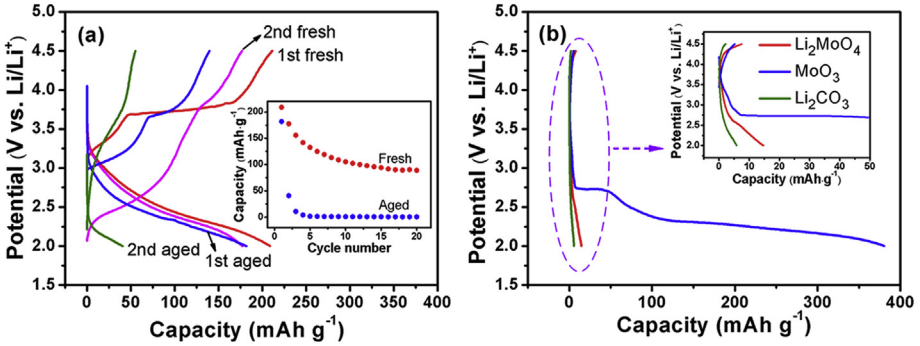


**Fig. 6.** (a) Charge and discharge potential curves of the fresh and aged $Li_2MoO_3$; the inset is for their cycling performances. (b) Initial charge and discharge curves of commercial $Li_2CO_3$, $MoO_3$ and $Li_2MoO_4$; the inset is for their selected potential curves between 0 and 50 mAh $g^{-1}$.

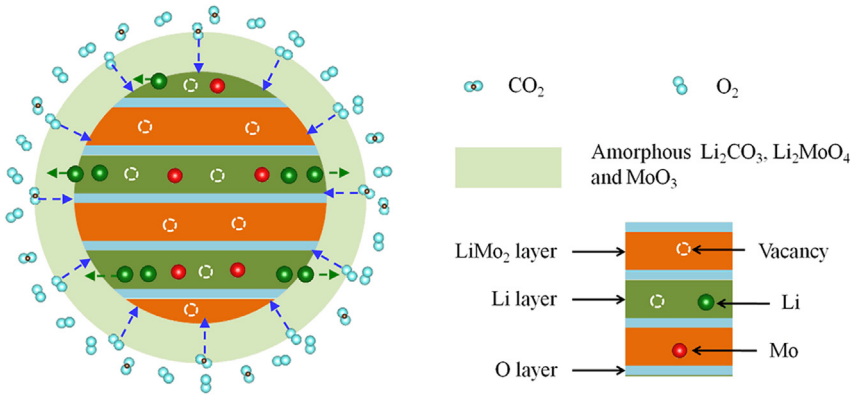


**Fig. 7.** A schematic illustration of the aging mechanism of $Li_2MoO_3$ in air.

$$Li_{2-2x}MoO_3 + (1-x)CO_2 + (1-x)/2O_2 \rightarrow (1-x)Li_2CO_3 + MoO_3 \quad (3)$$

Or the total reaction of $Li_2MoO_3$ in air can be written as

$$2Li_2MoO_3 + CO_2 + O_2 \rightarrow Li_2CO_3 + Li_2MoO_4 + MoO_3 \quad (4)$$

The above results show that $Li_2MoO_3$ can be oxidized/decomposed in air at room temperature and degraded in structural and electrochemical performances. These findings will shed light on the fabrication and application of $xLi_2MoO_3\cdot(1-x)LiM'O_2$ composite cathode materials. It must be pointed out, however, that the purpose of this work is to show the possibility of oxidation/decomposition of $Li_2MoO_3$ in air; the situation in reality will not be so severe for the following reasons. (1) The sample was stored in air for 120 days before testing, much longer than the time interval between material fabrication/packaging and battery assembly (one to two weeks). (2) The newly fabricated material is usually air-tightly packed before battery assembly; (3) $Li_2MoO_3$, like $Li_2MnO_3$, is usually not used as an independent cathode material. Rather, it is used to form a composite with $LiM'O_2$. Therefore, the number of $Mo^{4+}$ ions that are exposed to air is much smaller in a practical $xLi_2MoO_3\cdot(1-x)LiM'O_2$ composite than in $Li_2MoO_3$ alone. As a result, the $Mo^{4+}$ ions in $Li_2MoO_3$-based composite will have much less opportunity to be oxidized. Considering the high electric conductivity, its facile charge compensation by $Mo^{4+}/Mo^{6+}$ redox reaction instead of by oxygen evolution, and its structural and performance stability, $Li_2MoO_3$ is believed to be a promising building block for composing high-capacity Li-rich oxide cathode materials.

## 4. Conclusions

The surface of $Li_2MoO_3$ is demonstrated to be reactive towards $CO_2$ and $O_2$ in air at room temperature. It is partially oxidized/decomposed to amorphous $Li_2MoO_4$, $Li_2CO_3$ and $MoO_3$ after long-term storage in air at room temperature. Oxidation of the $Mo^{4+}$ ions and the consumption of the $Li^+$ ions lead to the creation of $Li^+$ vacancies, $Mo^{4+}$ ion migrations, Li–Mo antisites and destruction of $Mo_3O_{13}$ clusters in $Li_2MoO_3$. Therefore air exposure should try to be avoided in the fabrication and application of $Li_2MoO_3$. However, these reactions and structural/performance degradation are limited to a depth of less than 30 nm below the surface. Therefore, $Li_2MoO_3$ and its related compounds should be pretty stable towards air at room temperature. The findings on the reactivity of the Li-rich materials in air provide important insights into the fabrication, protection and applications of $xLi_2MoO_3\cdot(1-x)LiM'O_2$ composite cathode materials for lithium ion batteries though this work is focused on the stability of pure $Li_2MoO_3$ alone.

## Acknowledgments

This work was financially supported by the National Natural Science Foundation of China (NSFC No. 51372268) and National 973 Program of China (2009CB220100).

## References

[1] T.H. Kim, J.S. Park, S.K. Chang, S. Choi, J.H. Ryu, H.K. Song, Adv. Energy Mater. 2 (2012) 860–872.
[2] H.J. Yu, H.S. Zhou, J. Phys. Chem. Lett. 4 (2013) 1268–1280.
[3] C.S. Johnson, J.-S. Kim, C. Lefief, N. Li, J.T. Vaughey, M.M. Thackeray, Electrochem. Commun. 6 (2004) 1085–1091.
[4] M.M. Thackeray, S.-H. Kang, C.S. Johnson, J.T. Vaughey, R. Benedek, S.A. Hackney, J. Mater. Chem. 17 (2007) 3112–3125.
[5] A.R. Armstrong, M. Holzapfel, P. Novak, C.S. Johnson, S.-H. Kang, M.M. Thackeray, P.G. Bruce, J. Am. Chem. Soc. 128 (2006) 8694–8698.
[6] T. Ohzuku, M. Nagayama, K. Tsuji, K. Ariyoshi, J. Mater. Chem. 21 (2011) 10179–10188.
[7] J.-S. Kim, C.S. Johnson, M.M. Thackeray, Electrochem. Commun. 4 (2002) 205–209.
[8] J.-S. Kim, C.S. Johnson, J.T. Vaughey, M.M. Thackeray, S.A. Hackney, W. Yoon, C.P. Grey, Chem. Mater. 16 (2004) 1996–2006.
[9] M. Sathiya, K. Ramesha, G. Rousse, D. Foix, D. Gonbeau, A.S. Prakash, M.L. Doublet, K. Hemalatha, J.-M. Tarascon, Chem. Mater. 25 (2013) 1121–1131.
[10] M. Sathiya, G. Rousse, K. Ramesha, C.P. Laisa, H. Vezin, M.T. Sougrati, M.-L. Doublet, D. Foix, D. Gonbeau, W. Walker, A.S. Prakash, M. Ben Hassine, L. Dupont, J.-M. Tarascon, Nat. Mater. 12 (2013) 827–835.
[11] M.S. Park, J.W. Lee, W. Choi, D. Im, S.G. Doo, K.S. Park, J. Mater. Chem. 20 (2010) 7208–7213.
[12] H. Kobayashi, M. Tabuchi, M. Shikano, Y. Nishimura, H. Kageyama, T. Ishida, H. Nakamura, Y. Kurioka, R. Kanno, J. Power Sources 81–82 (1999) 524–529.
[13] A.C.W.P. James, J.B. Goodenough, J. Solid State Chem. 76 (1988) 87–96.
[14] S.J. Hibble, I.D. Fawcett, Inorg. Chem. 34 (1995) 500–508.
[15] S.J. Hibble, A.C. Hannon, I.D. Fawcett, J. Phys. Condens. Matter 11 (1999) 9203–9219.
[16] V. Pralong, Prog. Solid State Chem. 37 (2009) 262–277.
[17] M.S. Park, Y.G. Lim, J.H. Kim, K.J. Kim, J. Cho, J.S. Kim, Adv. Energy Mater. 1 (2011) 1002–1006.
[18] X. Xia, Z.X. Wang, L.Q. Chen, Electrochem. Commun. 10 (2008) 1442–1444.
[19] S. Hamelet, P. Gibot, M. Casas-Cabanas, D. Bonnin, C.P. Grey, J. Cabana, J.B. Leriche, J. Rodriguez-Carvajal, M. Courty, S. Levasseur, P. Carlach, M.V. Thournout, J.M. Tarascon, C. Masquelier, J. Mater. Chem. 19 (2009) 3979–3991.
[20] M. Cuisinier, J.F. Martin, N. Dupre, A. Yamada, R. Kanno, D. Guyomard, Electrochem. Commun. 12 (2010) 238–241.
[21] W. Porcher, P. Moreau, B. Lestriez, S. Jouanneau, D. Guyomard, Electrochem. Solid-State Lett. 11 (2008) A4–A8.
[22] G.V. Zhuang, G.Y. Chen, J. Shim, X.Y. Song, P.N. Ross, T.J. Richardson, J. Power Sources 134 (2004) 293–297.
[23] Y.J. Zhao, S.J. Wang, W.F. Ren, R. Wu, J. Electrochem. Soc. 160 (2013) A82–A86.
[24] K. Matsumoto, R. Kuzuo, K. Takeya, A. Yamanaka, J. Power Sources 81–82 (1999) 558–561.
[25] Y.R. Gao, Z.X. Wang, L.Q. Chen, J. Power Sources 245 (2014) 684–690.
[26] H. Wulff, M. Mohan Rao, F. Scholz, Chem. Mater. 15 (2003) 988–993.
[27] N. Tran, L. Croguennec, C. Jordy, Ph. Biensan, C. Delmas, Solid State Ionics 176 (2005) 1539–1547.
[28] H. Takeuchi, M. Arakawa, J. Phys. Soc. Jpn. 52 (1983) 279–283.
[29] Y.H. Li, S. Ishihara, J. Asian Earth Sci. 70–71 (2013) 142–159.
[30] M. Anwar, C.A. Hogarth, R. Bulpett, J. Mater. Sci. 24 (1989) 3087–3090.

[31] J.G. Choi, L.T. Thompson, Appl. Surf. Sci. 93 (1996) 143–149.
[32] J. Gopalakrishnan, V. Bhat, Mater. Res. Bull. 22 (1987) 769–774.
[33] H. Jezlorowskl, H. Knozinger, J. Phys. Chem. 83 (1979) 1166–1173.
[34] C. Kongmark, V. Martis, A. Rubbens, C. Pirovano, A. Lofberg, G. Sankar, E. Borders-Richard, R.-N. Vannier, W.V. Beek, Chem. Commun. 32 (2009) 4850–4852.
[35] H. Hu, I.E. Wachs, S.R. Bare, J. Phys. Chem. 99 (1995) 10897–10910.
[36] S. Sharma, R.N.P. Choudhary, J. Mater. Sci. Lett. 18 (1999) 669–672.
[37] R. Wang, X.Q. Yu, J.M. Bai, H. Li, X.J. Huang, L.Q. Chen, X.Q. Yang, J. Power Sources 218 (2012) 113–118.